Global inventory of nitrogen oxide emissions constrained by space-based observations of NO_2 columns

Randall V. Martin[1]
Harvard-Smithsonian Center for Astrophysics, Cambridge, Massachusetts, USA

Daniel J. Jacob
Division of Engineering and Applied Sciences, Harvard University, Cambridge, Massachusetts, USA

Kelly Chance and Thomas P. Kurosu
Harvard-Smithsonian Center for Astrophysics, Cambridge, Massachusetts, USA

Paul I. Palmer and Mathew J. Evans
Division of Engineering and Applied Sciences, Harvard University, Cambridge, Massachusetts, USA

Received 27 January 2003; revised 26 March 2003; accepted 7 April 2003; published 5 September 2003.

[1] We use tropospheric NO_2 columns from the Global Ozone Monitoring Experiment (GOME) satellite instrument to derive top-down constraints on emissions of nitrogen oxides ($NO_x \equiv NO + NO_2$), and combine these with a priori information from a bottom-up emission inventory (with error weighting) to achieve an optimized a posteriori estimate of the global distribution of surface NO_x emissions. Our GOME NO_2 retrieval improves on previous work by accounting for scattering and absorption of radiation by aerosols; the effect on the air mass factor (AMF) ranges from +10 to −40% depending on the region. Our AMF also includes local information on relative vertical profiles (shape factors) of NO_2 from a global 3-D chemical transport model (GEOS-CHEM); assumption of a globally uniform shape factor, as in most previous retrievals, would introduce regional biases of up to 40% over industrial regions and a factor of 2 over remote regions. We derive a top-down NO_x emission inventory from the GOME data by using the local GEOS-CHEM relationship between NO_2 columns and NO_x emissions. The resulting NO_x emissions for industrial regions are aseasonal, despite large seasonal variation in NO_2 columns, providing confidence in the method. Top-down errors in monthly NO_x emissions are comparable with bottom-up errors over source regions. Annual global a posteriori errors are half of a priori errors. Our global a posteriori estimate for annual land surface NO_x emissions (37.7 Tg N yr^{-1}) agrees closely with the GEIA-based a priori (36.4) and with the EDGAR 3.0 bottom-up inventory (36.6), but there are significant regional differences. A posteriori NO_x emissions are higher by 50–100% in the Po Valley, Tehran, and Riyadh urban areas, and by 25–35% in Japan and South Africa. Biomass burning emissions from India, central Africa, and Brazil are lower by up to 50%; soil NO_x emissions are appreciably higher in the western United States, the Sahel, and southern Europe. *INDEX TERMS:* 0345 Atmospheric Composition and Structure: Pollution—urban and regional (0305); 0365 Atmospheric Composition and Structure: Troposphere—composition and chemistry; 0394 Atmospheric Composition and Structure: Instruments and techniques; 1640 Global Change: Remote sensing; *KEYWORDS:* emissions, GOME, nitrogen oxides, biomass burning, retrieval, remote sensing

Citation: Martin, R. V., D. J. Jacob, K. Chance, T. P. Kurosu, P. I. Palmer, and M. J. Evans, Global inventory of nitrogen oxide emissions constrained by space-based observations of NO_2 columns, *J. Geophys. Res.*, *108*(D17), 4537, doi:10.1029/2003JD003453, 2003.

1. Introduction

[2] Nitrogen oxide radicals ($NO_x \equiv NO + NO_2$) originating from combustion, lightning, and soils largely control tropospheric ozone production [*Kasibhatla et al.*, 1991; *Penner et al.*, 1991; *Murphy et al.*, 1993; *Jacob et al.*, 1996]. Tropospheric ozone plays a key role in determining the oxidizing power of the atmosphere, is an important greenhouse gas, and is toxic to biota. "Bottom-up" inventories of NO_x emissions,

[1]Now at Department of Physics and Atmospheric Science, Dalhousie University, Halifax, Nova Scotia, Canada.

0148-0227/03/2003JD003453$09.00

based on limited knowledge of emission factors and extrapolation, are subject to substantial uncertainties [e.g., *Streets et al.*, 2003]. We show here that "top-down" information derived from space-based observations of NO_2 columns can reduce significantly the uncertainties in NO_x emissions when combined with a bottom-up inventory.

[3] The Global Ozone Monitoring Experiment (GOME) instrument on board the European Remote Sensing-2 satellite provides the capability for continuous global monitoring of NO_2 atmospheric columns through observation of solar backscatter [*European Space Agency*, 1995; *Thomas et al.*, 1998; *Burrows et al.*, 1999]. The satellite was launched in April 1995 into a Sun-synchronous orbit, crossing the equator at 1030 LT in the descending node. The GOME instrument observes the atmosphere in the nadir view with a surface spatial resolution of 40 km latitude by 320 km longitude in the forward scan, using a scanning mirror to measure three such scenes across the flight track. Global coverage is achieved every 3 days after 43 orbits.

[4] Several groups including our own have retrieved and interpreted tropospheric NO_2 columns from GOME [*Leue et al.*, 2001; *Velders et al.*, 2001; *Lauer et al.*, 2002; *Martin et al.*, 2002b; *Richter and Burrows*, 2002]. The retrieval involves three steps: (1) determining total NO_2 line-of-sight (slant) columns by spectral fitting of solar backscatter measurements, (2) removing the stratospheric columns by using data from remote regions where the tropospheric contribution to the column is small, and (3) applying an air mass factor (AMF) for the scattering atmosphere to convert tropospheric slant columns into vertical columns. The more recent algorithms [*Lauer et al.*, 2002; *Martin et al.*, 2002b; *Richter and Burrows*, 2002] explicitly remove an artifact thought to be introduced by the diffuser plate on the GOME instrument. Our previous AMF calculation described by *Martin et al.* [2002b] improved on earlier work by applying accurate surface reflectivities obtained from GOME measurements at appropriate wavelengths [*Koelemeijer et al.*, 2003], accounting for scattering by clouds, and resolving the spatial and temporal variability in the vertical profile of NO_2.

[5] Aerosols introduce an additional complication in the AMF calculation, enhancing or reducing the instrument sensitivity depending on the aerosol single-scattering albedo and its vertical distribution relative to the trace gas [*Palmer et al.*, 2001]. Previous NO_2 retrievals used a maritime aerosol distribution [*Velders et al.*, 2001; *Lauer et al.*, 2002; *Richter and Burrows*, 2002] or neglected the aerosols altogether [*Leue et al.*, 2001; *Martin et al.*, 2002b]. The present work improves on these retrievals by accounting for spatial and temporal variability of the aerosol, its multicomponent character, and its correlation with the NO_2 vertical profile.

[6] We go on to exploit the GOME tropospheric NO_2 column as a constraint toward improving NO_x emission inventories. In a pioneering study, *Leue et al.* [2001] used the GOME observations, together with an assumed constant NO_x lifetime of 27 hours estimated from GOME observations in continental outflow regions, to derive global NO_x emissions by mass balance. Their NO_x emission inventory showed major anomalies relative to bottom-up estimates, with larger emissions from Africa than from North America and Europe combined, likely due to errors in the AMF calculation and in the NO_x lifetime. Clearly, one cannot ignore the information from bottom-up NO_x inventories, which represent a considerable level of knowledge, and are broadly consistent with atmospheric observations when implemented in global models [i.e., *Emmons et al.*, 1997; *Horowitz et al.*, 1998; *Thakur et al.*, 1999; *Staudt et al.*, 2003]. Our inventory integrates information from bottom-up inventories and the top-down GOME observations, weighted by their respective errors, to optimize the use of the GOME data for constraining NO_x emissions.

2. Global Ozone Monitoring Experiment (GOME) Tropospheric NO_2 Retrieval With Aerosol Correction

[7] Our retrieval of tropospheric NO_2 columns presented here extends the July 1996 retrieval of *Martin et al.* [2002b] to an entire year, and accounts for the effects of aerosols on the AMF. We focus on the period September 1996–August 1997 during which satellite data including Along Track Scanning Radiometer (ATSR) firecounts and the Total Ozone Mapping Spectrometer (TOMS) Absorbing Aerosol Index constrain biomass burning emissions of aerosols and trace gases, and the large fires in Oceania associated with the 1997–1998 El Niño have not yet begun [*Duncan et al.*, 2003].

2.1. General Retrieval

[8] Following *Martin et al.* [2002b] we determine total slant columns of NO_2 by directly fitting backscattered radiance spectra observed by GOME over the wavelength region 423–451 nm. The stratospheric column and instrument biases are removed by assuming that NO_2 over the central Pacific is mainly stratospheric, subtracting the corresponding columns from the ensemble of GOME observations for the appropriate latitude, scan angle, and day of observation, and correcting the result for the small amount of tropospheric NO_2 over the Pacific. The stratospheric column is taken to be zonally invariant; this assumption does not cause significant error in summer [*Martin et al.*, 2002b], but is questionable north of 45°N in other seasons due to dynamical variability [*Douglass et al.*, 2001].

[9] We apply the AMF formulation of *Palmer et al.* [2001] to convert the resulting tropospheric slant columns into vertical columns. This formulation computes the AMF as the integral over the tropospheric column of the relative vertical distribution of NO_2 (shape factor) weighted by the local sensitivity to NO_2 of the solar radiation backscattered to space (scattering weights). The shape factor for every GOME scene is specified from a global 3-D model simulation of that scene (Goddard Earth Observing System, (GEOS)-CHEM model, see Appendix A), while the scattering weights are calculated from the Linearized Discrete Ordinate Radiative Transfer (LIDORT) model [*Spurr et al.*, 2001]. *Martin et al.* [2002b] improved the original AMF formulation of *Palmer et al.* [2001] to use local monthly mean surface reflectivity retrieved from GOME [*Koelemeijer et al.*, 2003] and to account for cloud scattering in partly cloudy scenes using local cloud information also retrieved from GOME [*Kurosu et al.*, 1999]. Here we further improve on the AMF formulation by accounting for extinction by aerosols as described in section 2.2 and by performing the radiative transfer calculation for each GOME scene rather than interpolating over a table of parameters. We exclude scenes in which more than 50% of the backscattered intensity is from the cloudy

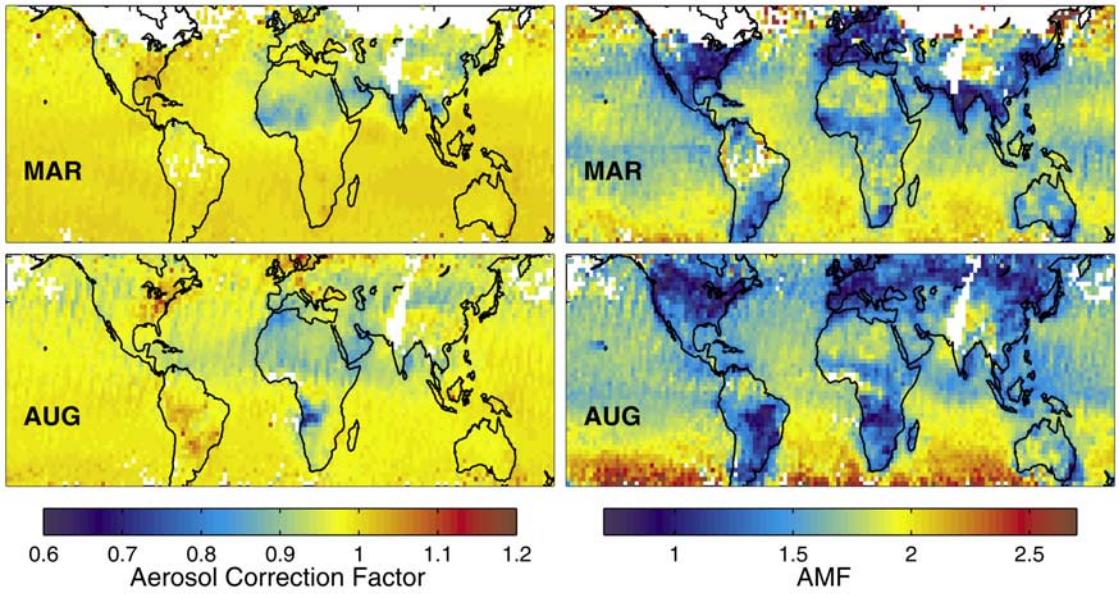

Figure 1. (right) Air mass factor (AMF) for conversion of slant to vertical tropospheric NO_2 columns in the Global Ozone Monitoring Experiment (GOME) measurements. Values are monthly means for March and August 1997. The AMF accounts for aerosol effects as described in section 2.2. There are no GOME data for the open area over central Asia; other open areas are regions of persistent snow cover or clouds. (left) Aerosol correction factor relative to an AMF calculation without aerosol effects, as by *Martin et al.* [2002b]. Values are shown between 40°S and 60°N, a region that comprises 99% of global NO_x emissions.

sky fraction of the scene as determined from the radiative transfer calculation constrained with the local cloud information. This threshold removes scenes with greater than about 40% cloud or snow cover.

2.2. Aerosol Correction

[10] We account for aerosols in the AMF calculation by representing their vertically resolved optical properties within the LIDORT model. Aerosol data retrieved from GOME are insufficient to constrain the AMF calculation due to lack of information about single scattering albedo [*Martin*, 2002]. Instead, we use monthly mean fields of aerosol mass concentration for September 1996–August 1997 from the Global Ozone Chemistry Aerosol Radiation and Transport (GOCART) model [*Chin et al.*, 2000a, 2002; *Ginoux et al.*, 2001]. These fields include sulfate, size-resolved mineral dust and sea salt, hydrophobic and hydrophilic black carbon, and hydrophobic and hydrophilic organic carbon. Extensive evaluations of the GOCART simulation with in situ and satellite observations have been presented in a number of papers [*Chin et al.*, 2000b, 2002; *Ginoux et al.*, 2001]. The same aerosol fields used here in the aerosol correction to the AMF are also used to account for the effect of aerosols on photolysis frequencies and heterogeneous chemistry in the GEOS-CHEM model [*Martin et al.*, 2003]. Aerosol optical properties including scattering phase function, single scattering albedo, vertically resolved optical thickness, and local hygroscopic growth factors are specified for each aerosol type following *Martin et al.*[2003].

[11] Figure 1 (left) shows the global distribution of the aerosol correction factors to the AMF for March and August 1997. Aerosols reduce the AMF by up to 40% over the biomass burning regions of India and central Africa, largely due to obscuration of the NO_2 column by black carbon with smaller contributions from organic carbon and mineral dust. The TOMS aerosol index [*Herman et al.*, 1997; *Torres et al.*, 1998] and in situ measurements [*Kuhlbusch et al.*, 1996; *Chowdhury et al.*, 2001] show high concentrations of absorbing aerosols over these regions. Aerosols reduce the AMF by 10–20% in dusty regions such as the Sahara, the northern tropical Atlantic Ocean, and the Middle East. By contrast, aerosols increase the AMF by 5–10% over industrial regions such as the eastern United States where scattering sulfate and organic aerosols dominate.

[12] Figure 1 (right) shows the AMF including the aerosol correction. Values are generally in the range of 0.8–1.5 over land and 1.5–2.5 over oceans, reflecting a larger relative contribution of the boundary layer to the tropospheric NO_2 column over land. However, relatively high AMFs are found over continental regions that are arid (deep boundary layer and high surface reflectivity), intensely convective, or snow covered. The seasonal variation in the AMF over the high-latitude oceans arises largely from the seasonal variation in solar zenith angle. The seasonal variation in the AMF over land is less pronounced except for regions of biomass burning.

[13] *Martin et al.* [2002b] showed that the total error in the retrieval of tropospheric NO_2 columns over continental source regions is largely determined by the AMF calculation. They derived through propagation of errors an overall error of 53% on the AMF calculation including contributions from errors in surface reflectivity (28%), the NO_2 profile (15%),

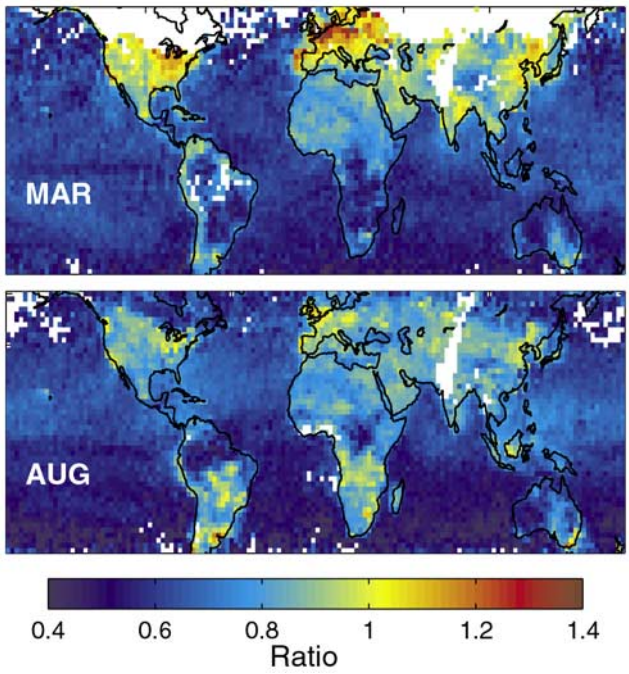

Figure 2. Contribution of the GEOS-CHEM relative vertical profiles of NO_2 concentrations (shape factor) to the AMF calculation. Shown is the ratio of the AMF calculated with a single NO_2 shape factor (uniform mixing ratio in the lowest 1.5 km and exponential decrease above with a scale height of 0.6 km) to the AMF calculated with local GEOS-CHEM NO_2 shape factors.

aerosols (30%), cloud cover (28%), and radiative transfer (10%). Our accounting for aerosols in the present work reduces the corresponding error by at least a factor of 2. The error from clouds is reduced to about 20% by retaining only scenes in which more than 50% of the backscattered radiation is from the clear-sky scene. The overall error in the AMF for each scene is now estimated to be 42%, and surface reflectivity is its single largest contributor. The error in the NO_2 retrieval due to spectral fitting and determination of the tropospheric column is about 1×10^{15} molecules cm^{-2} and dominates the overall retrieval error over the oceans and remote continental regions [*Martin et al.*, 2002b].

2.3. Sensitivity of the Air Mass Factor to the NO_2 Shape Factor

[14] Most GOME NO_2 retrievals have assumed a globally uniform shape factor [*Leue et al.*, 2001; *Velders et al.*, 2001; *Lauer et al.*, 2002; *Richter and Burrows*, 2002], which leads to bias in the retrieval [*Martin et al.*, 2002b] and presents difficulty when comparing retrieved and modeled columns, as the model may have in general a different shape factor than assumed in the retrieval [*Palmer et al.*, 2001]. (Comparing retrieved and modeled "slant" columns would only displace the problem.) Our approach has been to use local shape factors from the GEOS-CHEM global 3-D model of tropospheric chemistry, both to optimize the retrieval and to enable subsequent comparison of modeled and observed columns [*Palmer et al.*, 2001; *Martin et al.*, 2002b]. However, a concern is that the retrieval then contains model information that is not transparent.

[15] Figure 2 illustrates the model contribution to the retrieval by comparing the AMF calculated for a globally uniform shape factor with that calculated using NO_2 shape factors from the GEOS-CHEM model (the AMFs in this comparison do not include aerosol effects). *Martin et al.* [2002b] show an example of the contrast between model shape factors over land and ocean. The globally uniform shape factor assumes a uniform mixing ratio in the lowest 1.5 km, decreasing exponentially above with a scale height of 0.6 km, similar to that used in previous retrievals [*Leue et al.*, 2001; *Velders et al.*, 2001; *Lauer et al.*, 2002; *Richter and Burrows*, 2002]. The AMFs calculated with the globally uniform shape factor are about a factor of 2 lower than those calculated using GEOS-CHEM shape factors over remote regions, where actual NO_2 columns include a large contribution from the free troposphere. Previous reports of NO_2 plumes over the Atlantic Ocean from biomass burning or lightning [*Spichtinger et al.*, 2001; *Richter and Burrows*, 2002] could thus be biased high. Over industrial regions the AMFs calculated from the uniform profile are usually within 10% of the GEOS-CHEM values in summer, but up to 40% too high in March when the vertical mixing of surface emissions extends to less than 1.5 km altitude.

2.4. Global Distribution of NO_2 Columns

[16] Figure 3 (left) shows the seasonally averaged tropospheric NO_2 vertical columns retrieved from GOME. As mentioned above, scenes where clouds or snow dominate solar backscatter have been excluded from the average in order to reduce the retrieval error. The resulting bias is insignificant. Including these scenes would change the averages by less than 5×10^{14} molecules cm^{-2}, less than the fitting error. The NO_2 columns over industrial source regions are lowest in the summer due to rapid loss by reaction with OH [*Velders et al.*, 2001]. Seasonal enhancements from biomass burning are observed over northern Africa during December-January-February (DJF), India during March-April-May (MAM), and central Africa and South America from June to October. There are no evident enhancements along ocean ship tracks, but we have verified that this is not inconsistent with current ship emission inventories [*Corbett et al.*, 1999], which imply relatively low columns when averaged over a GOME scene. Regions of negative NO_2 columns over high-latitude oceans likely result from zonal variation in the stratospheric NO_2 column. Noise from the South Atlantic anomaly [*Heirtzler*, 2002] is observed near South America where GOME is exposed to increased radiation. Consistent with *Martin et al.* [2002b], we find no enhancements from lightning over tropical continental regions such as Central America and South Asia during summertime. Lightning makes little contribution (generally less than 4×10^{14} molecules cm^{-2} with local maxima of 9×10^{14} molecules cm^{-2}) to the NO_2 column during daytime [*Martin et al.*, 2002b; *Edwards et al.*, 2003], and therefore we would not expect to observe it from GOME.

3. Construction of a NO_x Emission Inventory

3.1. Strategy

[17] We construct here an optimized NO_x emission inventory by (1) inverting the GOME satellite observations of tropospheric NO_2 columns with the GEOS-CHEM model

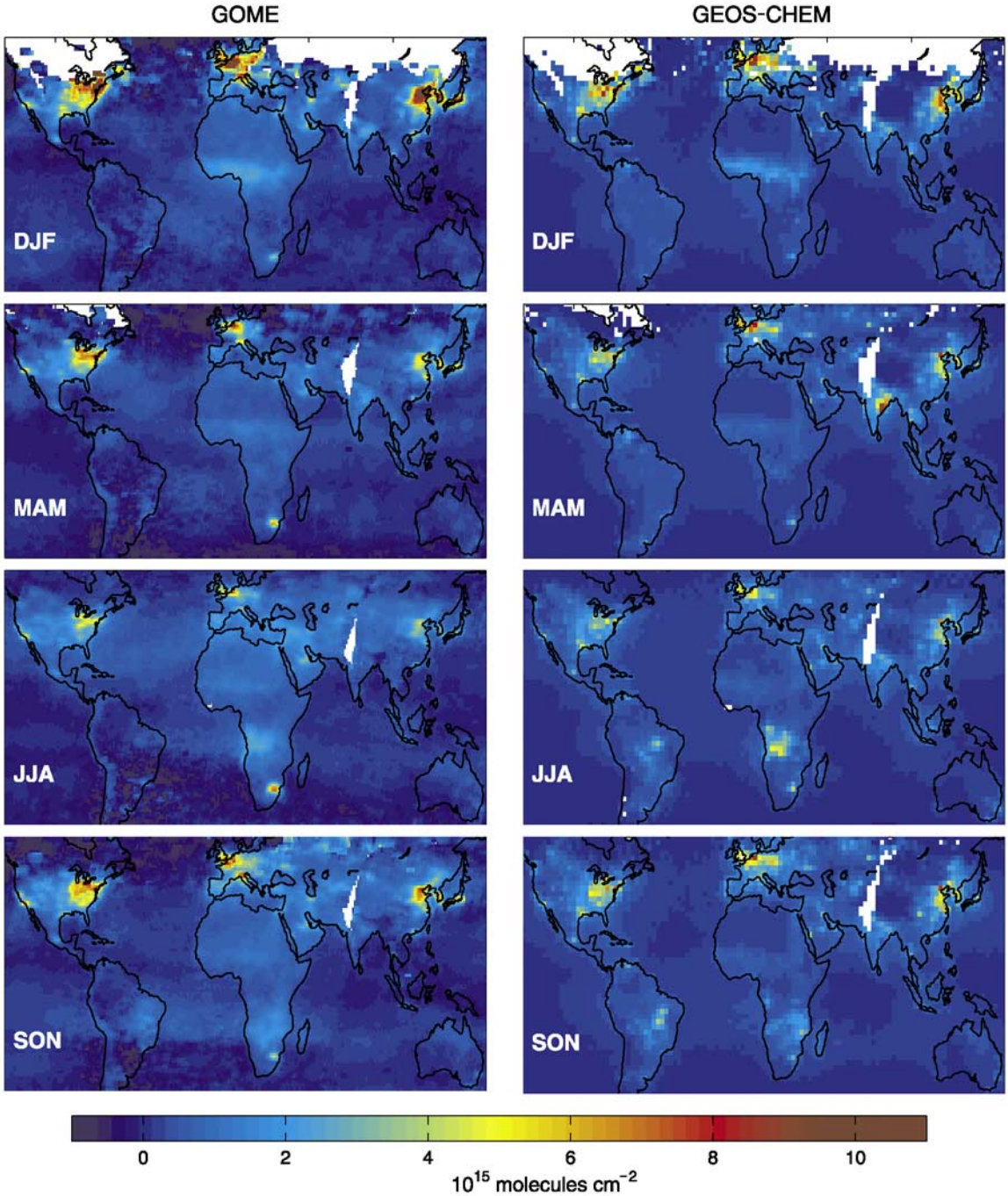

Figure 3. Seasonal mean tropospheric NO_2 columns for September 1996–August 1997. (left) GOME retrievals. (right) GEOS-CHEM model results sampled at the GOME overpass time. We capped the colorbar to highlight spatial structure; local retrieved NO_2 columns can approach 1.5×10^{16} molecules cm^{-2} over industrial regions during winter. The GEOS-CHEM model is described in Appendix A; NO_x emissions used in GEOS-CHEM are described in section 3.2.

and (2) combining the resulting top-down NO_x emission estimates with a priori estimates from a bottom-up inventory, weighted by the relative errors in the two estimates. From maximum likelihood, we express the monthly a posteriori emission, E (atoms N cm^{-2} s^{-1}), and its relative (geometric) error, ε, for a given location and month as a function of the a priori NO_x emission, E_a, the top-down NO_x emission, E_t, and the relative errors, ε_a and ε_t, on each. We assume a lognormal distribution of errors on E_a and E_t, so that maximum likelihood yields

$$\ln E = \frac{(\ln E_t)(\ln \varepsilon_a)^2 + (\ln E_a)(\ln \varepsilon_t)^2}{(\ln \varepsilon_a)^2 + (\ln \varepsilon_t)^2} \quad (1)$$

Table 1. A Priori GEOS-CHEM NO_x Emissions for September 1996–August 1997

Source	Emission Rate, Tg N yr^{-1}
Fossil fuel combustion	23.7
Lightning	6.2
Biomass burning	5.6
Soils	5.1
Biofuels	2.2
Aircraft	0.5
Stratosphere	0.1[a]

[a]The cross-tropopause NO_y flux is 0.5 Tg N yr^{-1} (including 0.1 Tg N yr^{-1} as NO_x and 0.4 Tg N yr^{-1} as HNO_3).

and

$$(\ln \varepsilon)^{-2} = (\ln \varepsilon_a)^{-2} + (\ln \varepsilon_t)^{-2}. \quad (2)$$

We apply this method to land surface emissions only, excluding lightning. Emissions of NO_x over ocean are very small and inferring them from the GOME data would be prone to excessive error. As discussed earlier, GOME NO_2 columns are insensitive to lightning NO_x emissions (most of the lightning NO_x in the upper troposphere is present as NO at 1030 LT of the GOME measurement [*Ridley et al.*, 1996]). An inventory that includes lightning would have ambiguous attribution of surface versus upper tropospheric emissions.

3.2. A Priori NO_x Emissions and NO_2 Columns

[18] The standard NO_x emission inventory used in the GEOS-CHEM model [*Bey et al.*, 2001a; *Martin et al.*, 2002a, 2003] is used here as the a priori. "Land surface sources here include contributions from fossil fuels, biofuels, biomass burning, and soils; it excludes contributions from lightning, aircraft, or the stratosphere. Table 1 contains the annual global NO_x emissions in GEOS-CHEM from all sources. Figure 4 (left) shows the spatial and seasonal variation of the land surface emissions. Anthropogenic NO_x emissions are from the Global Emission Inventory Activity (GEIA) [*Benkovitz et al.*, 1996] and are scaled to 1996–1997 as described by *Bey et al.* [2001a]. Soil NO_x emissions are computed locally using a modified version of the algorithm of *Yienger and Levy* [1995], as described by *Wang et al.* [1998]. Emissions from biofuels and biomass burning use the climatological combustion inventories of *Lobert et al.* [1999] for biomass burning and *Yevich and Logan* [2003] for biofuels; vegetation-specific emission factors are described by *Staudt et al.* [2003]. Biomass burning emissions are scaled to 1996–1997 and are distributed monthly on the basis of satellite observations [*Duncan et al.*, 2003].

[19] Evaluations of the GEOS-CHEM simulation with surface and aircraft observations for NO in different regions of the world have been presented in several papers [*Bey et al.*, 2001a, 2001b; *Fiore et al.*, 2002; *Martin et al.*, 2002a, 2002b]. The observations are sparse but are generally reproduced by the model to within a factor of 2. There is no indication of model bias in the vertical shape factor. Observations for NO_2 are even sparser but there is good confidence in the ability of models to simulate the observed NO/NO_2 ratio [*Bradshaw et al.*, 1999]. Figure 3 (right) shows the calculated tropospheric NO_2 columns in the GEOS-CHEM model using the NO_x emissions from Table 1 for the global distribution of monthly means. The model captures the seasonal enhancements over industrial regions during winter in the Northern Hemisphere and over South Africa. Most seasonal enhancements from biomass burning are larger in the model than observed by GOME. Mean model columns are 5% higher than retrieved by GOME and well correlated ($r = 0.75$, $n = 82{,}960$, $p < 0.005$).

[20] The top panel of Figure 5 and Table 2 show the specified error ε_a on the a priori inventory. We estimate the error in the fossil fuel and biofuel components of the a priori GEOS-CHEM inventory by comparison with the recently developed EDGAR 3.0 NO_x emission inventory for the year 1995 [*Olivier and Berdowski*, 2001]. The local ratio of GEOS-CHEM to EDGAR fossil fuel and biofuel emissions is taken as the relative error in these emissions; values are about 1.5 over much of the eastern United States and Europe. Annual global errors in biomass burning and soil NO_x emissions are about a factor of 3 [*Intergovernmental Panel on Climate Change*, 2001], and we adopt these values here. Local monthly errors may be much higher, but an error of a factor of 3 on the a priori is typically large relative to the error on the GOME top-down constraint so that accurate error specification is not important.

3.3. Top-Down Estimate of NO_x Emissions From GOME NO_2 Columns

[21] Top-down inference of an NO_x emission inventory E_t from the GOME NO_2 columns by mass balance [*Leue et al.*, 2001] requires at minimum three pieces of information: the retrieved tropospheric NO_2 column Ω_r, the ratio of tropospheric NO_x to NO_2 columns, and the NO_x lifetime τ_{NO_x} against loss to stable reservoirs. We obtain the latter two pieces of information from the GEOS-CHEM model. Mass balance for the NO_x column then yields a linear relationship between E_t and Ω_r:

$$E_t = \alpha \Omega_r, \quad (3)$$

where the linear coefficient $\alpha = (\Omega_{NO_x}/\Omega_{NO_2})/\tau_{NO_x}$ is determined by the GEOS-CHEM chemical mechanism and is to a first approximation independent of NO_x. The definition of τ_{NO_x} is complicated by rapid exchange of NO_x with peroxyacetylnitrates (PANs). We derive α here from the simulation with a priori emissions as $\alpha = E_a/\Omega_a$ where Ω_a is the NO_2 column from that simulation. This approach has the advantage of yielding an effective τ_{NO_x} that accounts for the complexities in NO_x chemistry and a $\Omega_{NO_x}/\Omega_{NO_2}$ ratio that accounts for free tropospheric sources as represented by the GEOS-CHEM model.

[22] In practice, τ_{NO_x} is mainly determined by the oxidation of NO_x to HNO_3 in the boundary layer. Horizontal transport of NO_x over this NO_x lifetime, which smears the local relationship between NO_2 columns and NO_x emissions, is a source of error in the application of equation (3). The NO_x loss to HNO_3 in the model is controlled largely by the OH + NO_2 reaction in the tropics and in the extratropics during summer, and by N_2O_5 hydrolysis on aerosol surfaces during extratropical winter. Figure 6 shows the zonal mean lifetime of NO_x against oxidation to HNO_3 in the continental boundary layer in different seasons. The lifetime is 3–10 hours, except in extratropical winter where it increases to 1–2 days. The

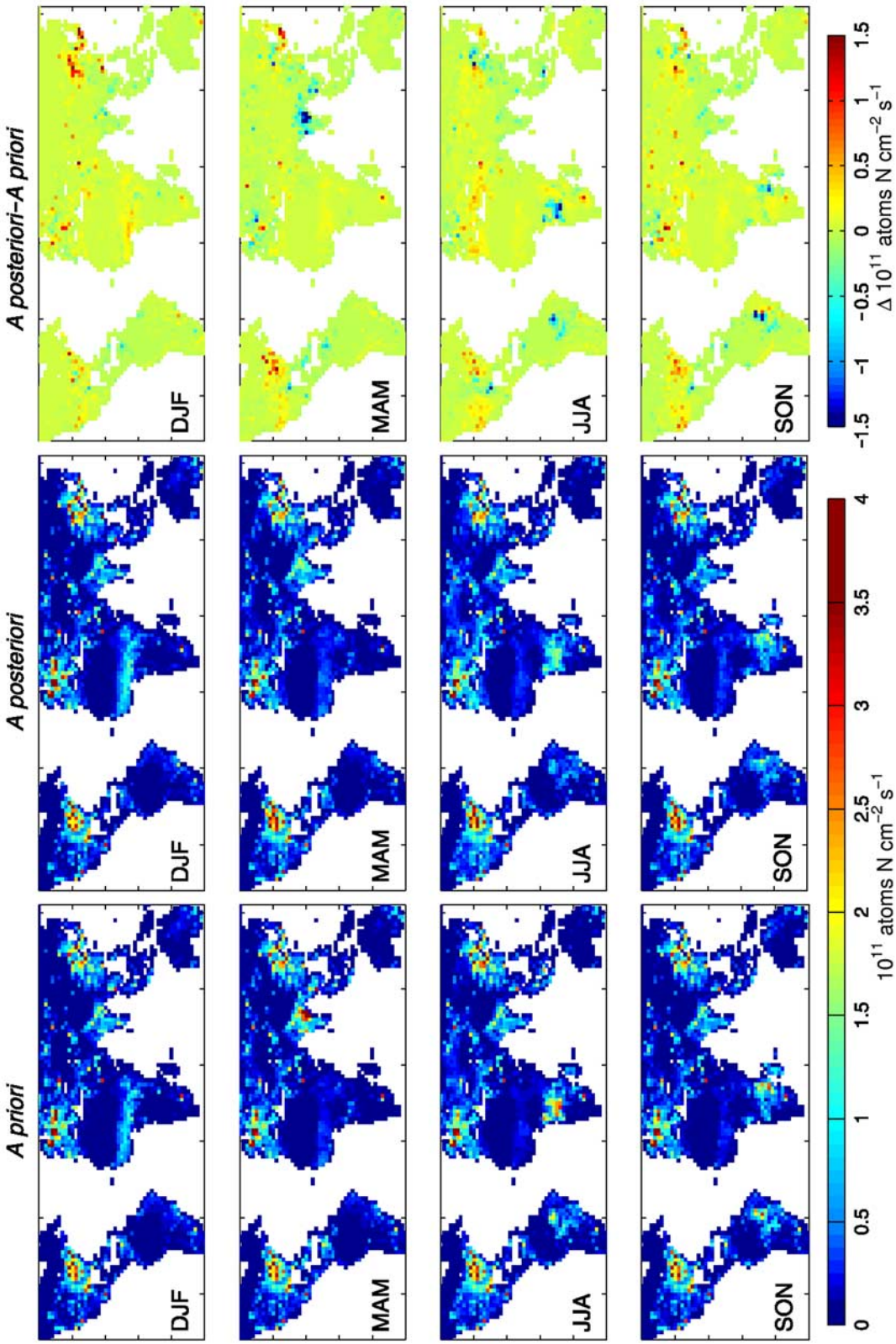

Figure 4. Seasonally averaged NO_x emissions from land with $2^\circ \times 2.5^\circ$ horizontal resolution: a priori (left), a posteriori (b, e, h, and k), and difference between the two (right). Only surface emissions are included; nonsurface emissions from lightning, aircraft, and the stratosphere are excluded. We capped the colorbar to highlight spatial structure; values as high as 8×10^{11} molecules cm^{-2} are found in some industrial regions.

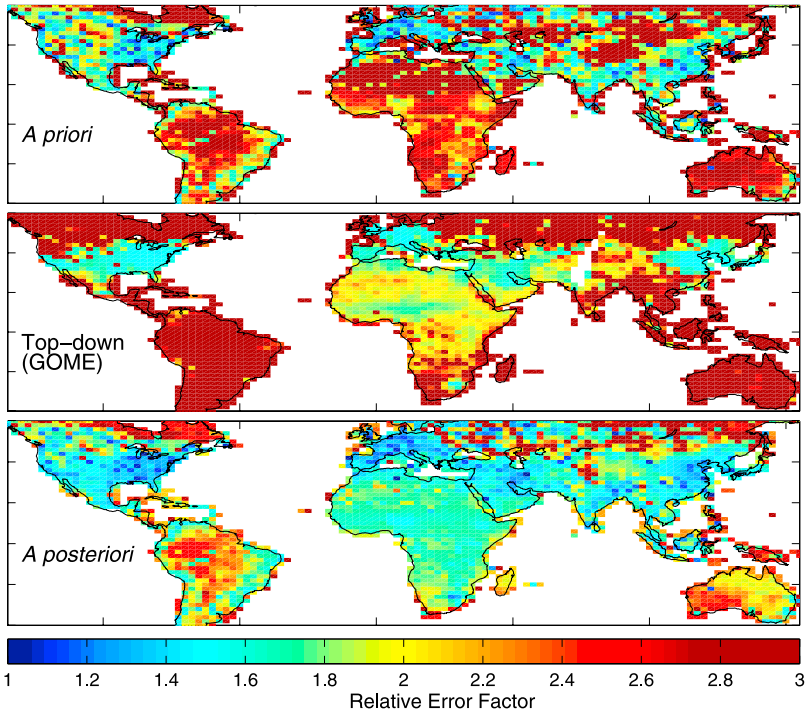

Figure 5. Relative annual mean error in the NO_x emission inventories. The relative error factor is the geometric standard deviation of the error. The a posteriori error is calculated from the a priori and GOME errors using equation (2). The colorbar is capped to highlight spatial structure; local error factors from GOME are very large over regions where retrieved tropospheric NO_2 columns are below the detection limit of 1×10^{15} molecules cm^{-2} (Figure 3).

corresponding smearing length scale [*Palmer et al.*, 2003] is ~100 km, on the same order as the GOME pixel size and the GEOS-CHEM model resolution; therefore we neglect smearing in our analysis. A more sophisticated inversion that accounts for NO_x transport would improve the inference of NO_x emissions from GOME observations during winter.

[23] The middle panel of Figure 5 and Table 2 show the annual mean error in top-down NO_x emissions determined

Table 2. Regional NO_x Emissions (and Relative Errors)[a]

	A priori	EDGAR[b]	GOME (Top-Down)	A Posteriori
United States	6.5(1.8)	6.1	8.3(1.7)	7.1(1.4)
Europe	5.6(2.0)	7.6	5.8(1.7)	5.9(1.5)
East Asia[c]	4.5(2.1)	5.1	4.7(1.7)	4.7(1.5)
Northern Africa	2.7(2.5)	2.7	4.0(1.9)	3.5(1.6)
South America	3.5(2.4)	2.9	2.2(2.7)	3.1(1.9)
South Asia (MAM)[d]	1.4(2.3)	0.73	0.67(2.0)	0.89(1.6)
South Asia (rest of the year)	2.3(2.0)	2.2	1.4(2.3)	2.1(1.7)
North Asia[e]	2.4(2.1)	2.0	2.9(2.0)	2.6(1.7)
Central Africa[f]	2.4(2.8)	1.5	2.3(1.9)	2.2(1.7)
Middle East[g]	1.5(2.0)	1.3	2.0(1.8)	1.7(1.5)
Australia[h]	1.4(2.6)	1.4	1.1(3.0)	1.4(2.0)
Central America	0.85(2.3)	0.60	0.60(2.4)	0.75(1.8)
Japan	0.47(2.9)	1.0	0.74(1.6)	0.64(1.5)
South Africa	0.45(2.1)	0.54	0.73(1.9)	0.57(1.6)
Canada	0.55(2.0)	0.83	0.48(2.9)	0.56(1.8)
Total	36.4(2.0)	36.6	38.0(2.0)	37.7(1.6)

[a]Units are Tg N yr^{-1}. Relative errors represent the geometric standard deviation about the expected value. Region boundaries follow standard convention. Values are annual means except for South Asia. They include all land surface sources (fossil fuel combustion, biofuels, biomass burning, and soils) and exclude nonsurface sources (lightning, aircraft, and the stratosphere).

[b]The EDGAR 3.0 inventory only includes industrial, biomass burning, and biofuel emissions. We add the GEOS-CHEM soil NO_x emissions here for consistency.

[c]East Asia here includes China and Korea, but not Japan.

[d]Totals for South Asia are shown separately for March-May (biomass burning season) and the rest of the year. South Asia here includes India and Southeast Asia. MAM, March-April-May.

[e]North Asia here extends poleward of 40°N and eastward of 43°E.

[f]Central Africa here spans 22°S to the equator.

[g]Middle East here covers 43°E–70°E and 12°N–40°N.

[h]Australia here includes the islands of Oceania south of the equator.

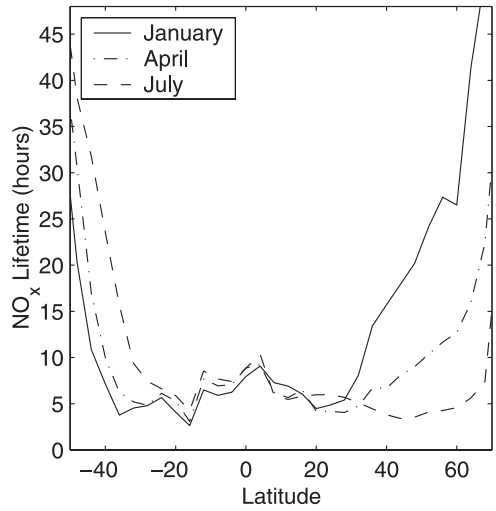

Figure 6. Zonal mean lifetime of NO_x against oxidation to HNO_3 in the boundary layer (0–2 km above surface), as calculated in the GEOS-CHEM model for January, April, and July. Values for October are similar to April. Oxidation of NO_x to HNO_3 in the model takes place mainly by the gas phase NO_2 + OH reaction and by hydrolysis of N_2O_5 in aerosols.

from GOME NO_2 columns. As discussed in section 2.2, the error in the retrieved NO_2 column includes an absolute error of 1×10^{15} molecules cm^{-2}, largely from the spectral fit, and a relative error of 42% from the AMF calculation. These errors were derived for individual retrievals, but we apply them to monthly mean fields to be conservative. If the retrieval errors are truly random, monthly mean errors would be 20% of the errors used here. Previous comparison of GEOS-CHEM model results with observations of the NO_x/NO_y concentration ratio over the United States [*Fiore et al.*, 2002] suggests that model error in the calculation of α adds another 30% error in quadrature to the mapping of NO_2 columns to NO_x emissions. The resulting relative errors in top-down emissions, shown in Figure 5, are 1.5 over continental source regions and higher elsewhere. Remote regions with negative monthly mean NO_2 columns (reflecting errors in spectral fitting or subtraction of the stratospheric column) are assigned a very large error and hence contain no top-down information. We see from Figure 5 that top-down errors are comparable with bottom-up errors over industrial regions, and are much smaller than bottom-up errors over the southwestern United States, the Middle East, parts of Asia, and Africa. Top-down errors exceed bottom-up errors over regions where retrieved columns are low and bottom-up emission estimates generally are low.

[24] Table 2 provides regional top-down emissions. The values for North America are within 20% of the GOME top-down inventory calculated by *Leue et al.* [2001], but there are large differences for the rest of the world. Top-down emissions for Africa, Australia, and South America are about half those reported by *Leue et al.* [2001], and emissions for Europe and East Asia are 50–75% higher. Treatment of the AMF and the NO_x lifetime likely explains the difference the two studies.

3.4. A Posteriori NO_x Emissions

[25] Figure 4 and Table 2 give the spatial distributions and regional totals of NO_x emissions for the a posteriori inventory (computed from equation (1)). Figure 5 and Table 2 show that the a priori and top-down information contribute nearly equally to the a posteriori in the global mean. Table 2 also includes regional totals from the EDGAR emission inventory. Global annual surface NO_x emissions in the a posteriori inventory are 37.7 Tg N yr^{-1}, not significantly different from the GEOS-CHEM a priori (36.4) or EDGAR 3.0 (36.6) values. Global annual errors are reduced from a factor of 2.0 for the a priori to 1.6 for the a posteriori. The monthly global a posteriori inventory is highly correlated with the a priori ($r^2 = 0.86$, $n = 35{,}568$), but there are some significant regional differences discussed below. We see from Figure 4 that there is little seasonal variation in a posteriori emissions from industrial regions of North America or Europe, where anthropogenic emissions (known to be largely aseasonal [*National Acid Precipitation Assessment Program*, 1991]) dominate. These regions show large seasonal variation in GOME NO_2 columns Ω_r, but Ω_r/τ_{NO_x} has in fact little seasonal variation, providing confidence in our approach.

[26] A posteriori NO_x emissions from the United States are 10% higher than the a priori inventory. A recent NO_x emission estimate [*Environmental Protection Agency*, 2000] suggests that the a priori US emissions used here for 1996–1997 are biased low by 20%, consistent with the information from GOME data. Differences between the a posteriori and a priori inventories in the western United States are largest in summer, which could reflect an underestimate of soil NO_x emissions in the a priori. Both a posteriori and EDGAR NO_x emissions are higher than the a priori inventory for Europe, by up to 50% in the polluted Po Valley of Italy. A posteriori emissions from southern Europe are largest during summer, again suggesting a contribution from soil NO_x emissions.

[27] The largest regional percentage increases in NO_x emissions from the a priori to the a posteriori are for the Middle East, northern Africa, South Africa, and Japan (Table 2). Figure 4 shows that much of the increase in NO_x emissions for the Middle East is from Riyadh and Tehran which are underestimated by 50–100% throughout the year. The increase in NO_x emissions for northern Africa represents a large percentage increase (25%) but a small absolute difference (0.8 Tg N yr^{-1}) over a large area. Most of the increase in NO_x emissions is from the Sahel throughout the year. The algorithm of *Yienger and Levy* [1995] for soil NO_x emissions used here as a priori may underestimate emissions from the Sahel by more than a factor of 2 [*Le Roux et al.*, 1995; *Davidson and Kingerlee*, 1997]. South African emissions are underestimated by 25%, largely due to emissions from the industrial Highveld plateau. Emissions from Japan are underestimated by 35%.

[28] Regional decreases for South Asia, South America, and central Africa between the a priori and the a posteriori emission inventories largely reflect biomass burning. Figure 4 shows local decreases of up to 50% for South Asia during March–May, and for South America and central Africa during July-October. In contrast, a posteriori emissions are higher over the northern African biomass burning region. Errors in the aerosol correction are insufficient to explain

these discrepancies [*Martin*, 2002]. Errors in NO_x emission inventories for biomass burning arise from estimates of biomass burned and of the NO_x emission factors (NO_x emitted per kg of dry matter burned). The NO_x emission factor for savannas is particularly uncertain (3.9 ± 2.4 g/kg) [*Andreae and Merlet*, 2001]. The NO_x emission factors used in the a priori inventory are 1.1 g/kg for northern African savannas and 3.9 g/kg for other savannas [*Staudt et al.*, 2003]. The a posteriori inventory suggests that NO_x emission factors may be more uniform across different savanna types and closer to the low end recommended by Andreae and Merlet. Analyses of CO observations from the MOPITT instrument (C. L. Heald et al., Transpacific satellite and aircraft observations of Asian pollution, submitted to *Journal of Geophysical Research*, 2003) and from the TRACE-P aircraft mission [*Palmer et al.*, 2003] are consistent with an overestimate of biomass burned in South Asia.

[29] A posteriori NO_x emissions from South Asia are 20% lower than the a priori during the biomass burning season of March-May, and 10% lower during the rest of the year when anthropogenic emissions dominate. The GOME NO_2 columns would suggest a greater reduction of emissions during the rest of the year, but have limited weight relative to the a priori due to high relative errors (Figure 5). An anthropogenic NO_x emission inventory for India [*Garg et al.*, 2001] gives a national estimate of half the a priori inventory used here, but this inventory does not completely account for emissions from biomass burning, biofuels, and soils.

[30] As shown in Table 2, a posteriori regional emission inventories tend to fall between the EDGAR 3.0 and a priori inventories. Regional totals in the a posteriori inventory are higher than the EDGAR inventory for central Africa (55%), northern Asia (30%), and the United States (20%). A posteriori NO_x emissions are lower than EDGAR emissions for Japan (40%), Canada (30%), and Europe (25%). The annual mean correlation r between EDGAR and the a posteriori inventory is 0.64 (n = 2964).

[31] Figure 5 shows that a posteriori errors are substantially lower than a priori errors throughout the world. Top-down information from GOME provides especially large error reductions over remote regions including Africa, the Middle East, South Asia, and the western United States. A posteriori errors over the eastern United States, Europe, and eastern China are typically less than 40%.

4. Conclusions

[32] We have retrieved global distributions of tropospheric NO_2 columns from solar backscatter measurements by the Global Ozone Monitoring Experiment (GOME) for September 1996–August 1997. Our retrieval improves upon that of *Martin et al.* [2002b] to account for aerosol effects. The air mass factor (AMF) calculation includes vertically resolved aerosol fields from a global aerosol model GOCART. Absorbing aerosols decrease the sensitivity of GOME to the NO_2 column over biomass burning regions by up to 40%. Scattering aerosols increase the sensitivity of GOME to NO_2 over the eastern United States by 5–10%.

[33] The AMF calculation in our retrieval uses relative vertical profiles (shape factors) of NO_2 from a global 3-D model of tropospheric chemistry (GEOS-CHEM). The GOME NO_2 retrievals carried out by other groups have assumed a globally uniform shape factor. We show that assuming a globally uniform shape factor introduces regional biases of up to 40% over industrial regions and a factor of 2 over remote regions.

[34] Retrieved NO_2 columns are lowest during summer, due to rapid loss by reaction with OH. Seasonal enhancements from biomass burning occur over northern Africa during DJF, over India during MAM, and over central Africa and South America during June-October. No enhancements are observed along ocean ship tracks, but this is not inconsistent with current ship emission inventories. No enhancements from lightning are observed over tropical continental regions, but again this is not inconsistent with current lightning emission estimates (most of the lightning NO_x in the upper troposphere is present as NO at 1030 LT of the GOME measurement).

[35] We used the GOME retrievals of NO_2 columns to derive monthly top-down constraints for NO_x emissions through inversion with the GEOS-CHEM model, and we combined these constraints with bottom-up inventories to obtain an optimized a posteriori estimate of NO_x emissions from fossil fuels, biofuels, biomass burning, and soils. The optimization was weighted by the respective local errors in bottom-up and top-down estimates. We estimated the local errors in bottom-up industrial emissions by comparing the GEOS-CHEM and EDGAR 3.0 NO_x emission inventories; these errors are on the order of 50%. Bottom-up errors over regions dominated by soils and biomass burning are taken to be a factor of 3. Top-down errors derived from formal error propagation are about 50% over continental source regions, comparable with the bottom-up errors. Our top-down estimates of NO_x emissions over industrial source regions show little seasonal variation, as higher NO_2 columns in winter are offset by longer NO_x lifetimes; this result is consistent with bottom-up knowledge and provides an important test of the top-down method.

[36] Global annual surface NO_x emission in our a posteriori inventory is 37.7 Tg N yr^{-1}, which is not significantly different from the GEOS-CHEM a priori (36.4) or EDGAR 3.0 (36.6) values. About half of the information in the a posteriori inventory is from the top-down approach. Global annual errors are reduced from a factor of 2.0 for the a priori to 1.6 for the a posteriori. Monthly and spatial variation in a priori and a posteriori emissions are highly correlated (r^2 = 0.86, n = 35,568), but there are some significant regional differences. A posteriori NO_x emissions are higher by 50–100% in the Po Valley, Tehran, and Riyadh urban areas, by 25–35% in Japan and South Africa, and by 10% in the United States. A priori soil NO_x emissions appear to be too low over the Sahel, the western United States, and southern Europe. A priori estimates are too high by up to 50% in biomass burning regions of India, central Africa, and Brazil. Noteworthy differences between the a posteriori and EDGAR inventories are that the EDGAR inventory is too low over central Africa (55%) and the United States (20%), but too high over Japan (40%) and Europe (25%). A posteriori errors on emission estimates are substantially lower than a priori errors throughout the world, especially over Africa, the Middle East, South Asia, and the western United States.

[37] Two major limitations of the current work are the coarse horizontal resolution of the GOME instrument and

the lack of direct validation of the tropospheric NO_2 column product. Top-down emission inventories will be improved with the next generation of instruments featuring higher spatial resolution that enables more accurate cloud and aerosol corrections; the Scanning Imaging Absorption spectrometer for Atmospheric Chartography (SCIAMACHY) [*Bovensmann et al.*, 1999] on board ENVISAT and the Ozone Monitoring Instrument (OMI) on board Aura. Application of daily retrieved aerosol fields would increase the accuracy of the aerosol correction. Inversion of NO_x emissions at a higher resolution will require a more formal inverse analysis to account for transport. The higher resolution measurements may enable observation of ship emissions over oceans. Coincident limb measurements from both platforms will enable better separation of the stratosphere and troposphere. Direct validation of satellite observations with in situ measurements and comparison with high-resolution, customized bottom-up inventories will be needed for further progress.

Appendix A: GEOS-CHEM Model Description

[38] The determination of NO_x emissions from GOME observations of tropospheric NO_2 columns requires independent information on the relationship of NO_2 columns to NO_x emissions. A global 3-D model of tropospheric chemistry is the best source of this information. The GEOS-CHEM model was initially described by *Bey et al.* [2001a]. Subsequent improvements are described by *Martin et al.* [2002b, 2003]. We use here GEOS-CHEM version 4.26 (http://www-as.harvard.edu/chemistry/trop/geos/) with improved treatment of aerosol photochemical effects and a few other updates as described by *Martin et al.* [2003]. The model is driven by assimilated meteorological data from the Goddard Earth Observing System (GEOS) of the NASA Data Assimilation Office. The meteorological data include 3-D fields updated every 3 hours for surface fluxes and mixing depths, and every 6 hours for other variables. The NO_x emission inventory is discussed in section 3.2. We use for this study the GEOS data for 1996–1997, available with a resolution of 2° latitude by 2.5° longitude and 46 sigma levels in the vertical extending up to 0.1 hPa. The five lowest levels are centered at 50, 250, 600, 1100, and 1700 m for a column based at sea level. For computational expedience in GEOS-CHEM the vertical levels above the lower stratosphere are merged, retaining a total of 26. We retain the original horizontal resolution.

[39] The GEOS-CHEM model includes a detailed simulation of tropospheric O_3-NO_x-hydrocarbon chemistry, originally described by *Horowitz et al.* [1998] and updated as described by several people [*Bey et al.*, 2001a; *Fiore et al.*, 2002; *Martin et al.*, 2002a, 2003]. Reactions in aerosols, including N_2O_5 hydrolysis (reaction probability 0.1), are described by *Jacob* [2000]. The chemical evolution of about 120 species is computed with a Gear solver [*Jacobson and Turco*, 1994]. Photolysis frequencies are computed using the Fast-J radiative transfer algorithm [*Wild et al.*, 2000], which includes Rayleigh scattering as well as Mie scattering by clouds and aerosols. Aerosol fields affecting radiation and heterogeneous chemistry are 3-D monthly means from a 1996–1997 simulation with the GOCART model [*Chin et al.*, 2000a, 2002; *Ginoux et al.*, 2001], which uses the same GEOS meteorological fields and transport algorithms as GEOS-CHEM.

[40] **Acknowledgments.** We are grateful to Robert Koelemeijer for providing the surface reflectivity data, and to Mian Chin and Paul Ginoux for providing the aerosol fields. This work was supported by the NASA Atmospheric Chemistry Modeling and Analysis Program. Additional support was provided by Smithsonian Institution internal funds. Randall V. Martin was supported by a National Defense and Engineering Graduate Fellowship.

References

Andreae, M. O., and P. Merlet, Emission of trace gases and aerosols from biomass burning, *Global Biogeochem. Cycles*, *15*, 955–966, 2001.

Benkovitz, C. M., M. T. Scholtz, J. Pacyna, L. Tarrason, J. Dignon, E. C. Voldner, P. A. Spiro, J. A. Logan, and T. E. Graedel, Global gridded inventories for anthropogenic emissions of sulfur and nitrogen, *J. Geophys. Res.*, *101*, 29,239–29,253, 1996.

Bey, I., D. J. Jacob, R. M. Yantosca, J. A. Logan, B. D. Field, A. M. Fiore, Q. Li, H. Y. Liu, L. J. Mickley, and M. G. Schultz, Global modeling of tropospheric chemistry with assimilated meteorology: Model description and evaluation, *J. Geophys. Res.*, *106*, 23,073–23,096, 2001a.

Bey, I., D. J. Jacob, J. A. Logan, and R. M. Yantosca, Asian chemical outflow to the Pacific: Origins, pathways and budgets, *J. Geophys. Res.*, *106*, 23,097–23,114, 2001b.

Bovensmann, H., J. P. Burrows, M. Buchwitz, J. Frerick, V. V. Rozanov, K. V. Chance, and A. P. H. Goede, SCIAMACHY: Mission objectives and measurement modes, *J. Atmos. Sci.*, *56*, 127–150, 1999.

Bradshaw, J., et al., Photofragmentation two-photon laser-induced fluorescence detection of NO_2 and NO: Comparison of measurements with model results based on airborne observations during PEM-Tropics A, *Geophys. Res. Lett.*, *26*, 471–474, 1999.

Burrows, J. P., et al., The Global Ozone Monitoring Experiment (GOME): Mission concept and first scientific results, *J. Atmos. Sci.*, *56*, 151–175, 1999.

Chin, M., R. B. Rood, S.-J. Lin, J. F. Muller, and A. M. Thompson, Atmospheric sulfur cycle simulated in the global model GOCART: Model description and global properties, *J. Geophys. Res.*, *105*, 24,671–24,687, 2000a.

Chin, M., D. Savoie, B. J. Huebert, A. R. Bandy, D. C. Thornton, T. S. Bates, P. K. Quinn, E. S. Saltsman, and W. J. De Bruyn, Atmospheric sulfur cycle in the global model GOCART: Comparison with field observations and regional budgets, *J. Geophys. Res.*, *105*, 24,689–24,712, 2000b.

Chin, M., et al., Tropospheric aerosol optical thickness from the GOCART model and comparisons with satellite and sunphotometer measurements, *J. Atmos. Sci.*, *59*, 461–483, 2002.

Chowdhury, Z., L. S. Hughes, L. G. Salmon, and G. R. Cass, Atmospheric particle size and composition measurements to support light extinction calculations over the Indian Ocean, *J. Geophys. Res.*, *106*, 28,597–28,606, 2001.

Corbett, J. J., P. S. Fischbeck, and S. N. Pandis, Global nitrogen and sulfur inventories for ocean-going ships, *J. Geophys. Res.*, *104*, 3457–3470, 1999.

Davidson, E., and W. Kingerlee, A global inventory of nitric oxide emissions from soils, *Nutr. Cycling Agroecosyst.*, *48*, 37–50, 1997.

Douglass, A., J. Gleason, and M. Chin, Sources of variability in the stratospheric column of nitrogen dioxide, paper presented at the International Association of Meteorology and Atmospheric Sciences, Int. Union of Geodesy and Geophys., Innsbruck, Austria, 2001.

Duncan, B. N., R. V. Martin, A. C. Staudt, R. Yevich, and J. A. Logan, Interannual and seasonal variability of biomass burning emissions constrained by satellite observations, *J. Geophys. Res.*, *108*(D2), 4100, doi:10.1029/2002JD002378, 2003.

Edwards, D. P., et al., Tropospheric ozone over the tropical Atlantic: A satellite perspective, *J. Geophys. Res.*, *108*(D8), 4237, doi:10.1029/2002JD002927, 2003.

Emmons, L. K., et al., Climatologies of NO_x and NO_y: A comparison of data and models, *Atmos. Environ.*, *31*, 1851–1904, 1997.

Environmental Protection Agency, National air pollutant emission trends, 1900–1998, *EPA 454/R-00-002*, 238 pp., Washington, D. C., 2000.

European Space Agency, *The GOME Users Manual*, edited by F. Bednarz, ESA publ. Div. SP-1182, ESTEC, Noordwijk, Netherlands, 1995.

Fiore, A. M., D. J. Jacob, I. Bey, R. M. Yantosca, B. D. Field, A. C. Fusco, and J. G. Wilkinson, Background ozone over the United States in summer: Origin, trend, and contribution to pollution episodes, *J. Geophys. Res.*, *107*(D15), 4275, doi:10.1029/2001JD000982, 2002.

Garg, A., P. R. Shukla, S. Bhattacharya, and V. K. Dadhwal, Sub-region (district) and sector level SO_2 and NO_x emissions for India: Assessment of inventories and mitigation flexibility, *Atmos. Environ.*, *35*, 703–713, 2001.

Ginoux, P., M. Chin, I. Tegen, J. M. Prospero, B. Holben, O. Dubovik, and S.-J. Lin, Sources and distributions of dust aerosols simulated with the GOCART model, *J. Geophys. Res.*, *106*, 20,255–20,274, 2001.

Heirtzler, J. R., The future of the South Atlantic anomaly and implications for radiation damage in space, *J. Atmos. Sol. Terr. Phys.*, *64*, 1701–1708, 2002.

Herman, J. R., P. K. Bhartia, O. Torres, C. Hsu, C. Seftor, and E. Celarier, Global distribution of UV-absorbing aerosols from Nimbus 7-TOMS data, *J. Geophys. Res.*, *102*, 16,911–16,922, 1997.

Horowitz, L. W., J. Y. Liang, G. M. Gardner, and D. J. Jacob, Export of reactive nitrogen from North America during summertime, *J. Geophys. Res.*, *103*, 13,451–13,476, 1998.

Intergovernmental Panel on Climate Change, *Climate Change 2001*, 881 pp., Cambridge Univ. Press, New York, 2001.

Jacob, D. J., Heterogeneous chemistry and tropospheric ozone, *Atmos. Environ.*, *34*, 2131–2159, 2000.

Jacob, D. J., et al., Origin of ozone and NO_x in the tropical troposphere: A photochemical analysis of aircraft observations over the South Atlantic basin, *J. Geophys. Res.*, *101*, 24,235–24,250, 1996.

Jacobson, M. Z., and R. P. Turco, SMVGEAR: A sparse-matrix, vectorized Gear code for atmospheric models, *Atmos. Environ.*, *28*, 273–284, 1994.

Kasibhatla, P. S., H. Levy, W. J. Moxim, and W. L. Chameides, The relative importance of stratospheric photochemical production on tropospheric NO_y levels: A model study, *J. Geophys. Res.*, *96*, 18,631–18,646, 1991.

Koelemeijer, R. B. A., J. F. de Haan, and P. Stammes, A database of spectral surface reflectivity in the range 335–772 nm derived from 5.5 years of GOME observations, *J. Geophys. Res.*, *108*(D2), 4070, doi:10.1029/2002JD002429, 2003.

Kuhlbusch, T. A. J., M. O. Andreae, H. Cachier, J. G. Goldammer, J.-P. Lacaux, R. Shea, and P. J. Crutzen, Black carbon formation by savanna fires: Measurements and implications for the global carbon cycle, *J. Geophys. Res.*, *101*, 23,651–23,665, 1996.

Kurosu, T. P., K. Chance, and R. J. D. Spurr, CRAG-cloud retrieval algorithm for ESA's global ozone monitoring experiment, *ESA WPP-161*, pp. 513–521, Eur. Space Res. and Tech Cent., Noordwijk, Netherlands, 1999.

Lauer, A., M. Dameris, A. Richter, and J. P. Burrows, Tropospheric NO_2 columns: A comparison between model and retrieved data from GOME measurements, *Atmos. Chem. Phys.*, *2*, 67–78, 2002.

Le Roux, X., L. Abbadie, R. Lensi, and D. Serca, Emissions of nitrogen monoxide from African tropical ecosystems: Control of emissions by soil characteristics in humid and dry savannas of West Africa, *J. Geophys. Res.*, *100*, 23,133–23,142, 1995.

Leue, C., M. Wenig, T. Wagner, O. Klimm, U. Platt, and B. Jahne, Quantitative analysis of NO_x emissions from GOME satellite image sequences, *J. Geophys. Res.*, *106*, 5493–5505, 2001.

Lobert, J. M., W. C. Keene, J. A. Logan, and R. Yevich, Global chlorine emissions from biomass burning: The reactive chlorine emissions inventory, *J. Geophys. Res.*, *104*, 8373–8390, 1999.

Martin, R. V., Satellite observations of tropospheric chemistry: Retrievals and interpretation, Ph.D. thesis, Harvard Univ., Cambridge, Mass., 2002.

Martin, R. V., et al., Interpretation of TOMS observations of tropical tropospheric ozone with a global model and in situ observations, *J. Geophys. Res.*, *107*(D18), 4351, doi:10.1029/2001JD001480, 2002a.

Martin, R. V., et al., An improved retrieval of tropospheric nitrogen dioxide from GOME, *J. Geophys. Res.*, *107*(D20), 4437, doi:10.1029/2001JD001027, 2002b.

Martin, R. V., D. J. Jacob, R. M. Yantosca, M. Chin, and P. Ginoux, Global and regional decreases in tropospheric oxidants from photochemical effects of aerosols, *J. Geophys. Res.*, *108*(D3), 4097, doi:10.1029/2002JD002622, 2003.

Murphy, D., D. Fahey, M. Proffitt, S. Liu, C. Eubank, S. Kawa, and K. Kelly, Reactive odd nitrogen and its correlation with ozone in the lower stratosphere and upper troposphere, *J. Geophys. Res.*, *98*, 8751–8773, 1993.

National Acid Precipitation Assessment Program, 1990 Integrated assessment report, 520 pp., Washington, D. C., 1991.

Olivier, J. G. J., and J. J. M. Berdowski, Global emissions sources and sinks, in *The Climate System*, edited by J. Berdowski, R. Guicherit, and B. J. Heij, pp. 33–78, A. A. Balkema Publ., Rotterdam, Netherlands, 2001.

Palmer, P. I., D. J. Jacob, K. Chance, R. V. Martin, R. J. D. Spurr, T. P. Kurosu, I. Bey, R. Yantosca, A. Fiore, and Q. Li, Air mass factor formulation for spectroscopic measurements from satellites: Application to formaldehyde retrievals from the Global Ozone Monitoring Experiment, *J. Geophys. Res.*, *106*, 14,539–14,550, 2001.

Palmer, P. I., D. J. Jacob, D. B. Jones, C. Heald, R. Yantosca, J. A. Logan, G. W. Sachse, and D. Streets, Inverting for emissions of carbon monoxide from Asia using aircraft observations over the western Pacific, *J. Geophys. Res.*, *108*, doi:10.1029/2003JD003397, in press, 2003.

Penner, J. E., C. S. Athertson, J. Dignon, S. J. Ghan, J. J. Walton, and S. Hameed, Tropospheric nitrogen: A three-dimensional study of sources, distributions, and deposition, *J. Geophys. Res.*, *96*, 959–990, 1991.

Richter, A., and J. P. Burrows, Tropospheric NO_2 from GOME measurements, *Adv. Space Res.*, *29*, 1673–1683, 2002.

Ridley, B. A., J. E. Dye, J. G. Walega, J. Zheng, F. E. Grahek, and W. Rison, On the production of active nitrogen by thunderstorms over New Mexico, *J. Geophys. Res.*, *101*, 20,985–21,005, 1996.

Spichtinger, N., M. Wenig, P. James, T. Wagner, U. Platt, and A. Stohl, Satellite detection of a continental-scale plume of nitrogen oxides from boreal forest fires, *Geophys. Res. Lett.*, *28*, 4579–4582, 2001.

Spurr, R. J. D., T. P. Kurosu, and K. V. Chance, A linearized discrete ordinate radiative transfer model for atmospheric remote sensing retrieval, *J. Quant. Spectrosc. Radiat. Transfer*, *68*, 689–735, 2001.

Staudt, A. C., F. Ravetta, J. A. Logan, D. Bachiochi, T. N. Krishnamurti, S. Sandholm, B. Ridley, H. B. Singh, and B. Talbot, Sources and chemistry of nitrogen oxides over the tropical Pacific, *J. Geophys. Res.*, *108*(D2), 8239, doi:10.1029/2002JD002139, 2003.

Streets, D., et al., An inventory of gaseous and primary aerosol emissions in Asia in the year 2000, *J. Geophys.*, *108*, doi:10.1029/2002JD003093, in press, 2003.

Thakur, A. N., H. B. Singh, P. Mariani, Y. Chen, Y. Wang, D. J. Jacob, G. Brasseur, J.-F. Müller, and M. Lawrence, Distribution of reactive nitrogen species in the remote free troposphere: Data and model comparisons, *Atmos. Environ.*, *33*, 1403–1422, 1999.

Thomas, W., E. Hegels, S. Slijkhuis, R. Spurr, and K. Chance, Detection of biomass burning combustion products in southeast Asia from backscatter data taken by the GOME spectrometer, *Geophys. Res. Lett.*, *25*, 1317–1320, 1998.

Torres, O., P. K. Bhartia, J. R. Herman, Z. Ahmad, and J. Gleason, Derivation of aerosol properties from satellite measurements of backscattered ultraviolet radiation: Theoretical basis, *J. Geophys. Res.*, *103*, 17,099–17,110, 1998.

Velders, G. J. M., C. Granier, R. W. Portmann, K. Pfeilsticker, M. Wenig, T. Wagner, U. Platt, A. Richter, and J. P. Burrows, Global tropospheric NO_2 column distributions: Comparing 3-D model calculations with GOME measurements, *J. Geophys. Res.*, *106*, 12,643–12,660, 2001.

Wang, Y., D. J. Jacob, and J. A. Logan, Global simulation of tropospheric O_3-NO_x-hydrocarbon chemistry: 1, Model formulation, *J. Geophys. Res.*, *103*, 10,713–10,726, 1998.

Wild, O., X. Zhu, and M. J. Prather, Fast-J: Accurate simulation of in- and below-cloud photolysis in tropospheric chemistry models, *J. Atmos. Chem.*, *37*, 245–282, 2000.

Yevich, R., and J. A. Logan, An assessment of biofuel use and burning of agricultural waste in the developing world, *Global Biogeochem. Cycles*, in press, 2003.

Yienger, J. J., and H. Levy, Empirical model of global soil-biogenic NO_x emissions, *J. Geophys. Res.*, *100*, 11,447–11,464, 1995.

K. Chance and T. P. Kurosu, Harvard-Smithsonian Center for Astrophysics, Cambridge, MA 02138, USA. (kchance@cfa.harvard.edu; tkurosu@cfa.harvard.edu)

M. J. Evans, D. J. Jacob, and P. I. Palmer, Division of Engineering and Applied Sciences, Harvard University, Cambridge, MA 02138, USA. (mje@io.harvard.edu; djj@io.harvard.edu; pip@io.harvard.edu)

R. V. Martin, Department of Physics and Atmospheric Science, Dalhousie University, Halifax, Nova Scotia, Canada B3H 3J5. (rvmartin@fizz.phys.dal.ca)